Modelling debris flow entrainment: analytical model, numerical experiment and case study

Chao Kang
MOE Key Laboratory of Mechanics on Disaster and Environment in Western China, School of Civil Engineering and Mechanics, Lanzhou University, Lanzhou 730000, Gansu, China
Department of Civil and Environmental Engineering, University of Alberta, Edmonton, Alberta, Canada
Peng Cui
Institute of Mountain Hazards & Environment, Chinese Academy of Science, Chengdu China.
Dave Chan
College of Civil Engineering and Architecture, Three Gorges University, Yichang, Hubei Province, China
Department of Civil and Environmental Engineering, University of Alberta, Edmonton, Alberta, Canada

ABSTRACT
Debris flows that entrain sediment by undermining channel beds or scouring channel banks can become exceptionally mobile and destructive. Therefore, the calculation of entrainment plays an important role in debris flow runout analysis. An entrainment model has been developed that takes into account surface erosional effects by considering progressive scouring on the channel bed. Newton's Law of Motion is used to calculate the acceleration, velocity, and displacement of the erodible material. To understand the entrainment process in granular flow, a flow channel of 8 m long with 15-degree slope is simulated using the Discrete Element Method (DEM). Results of the numerical experiment are compared with analytical calculations. The variation of the depth and the rate of erosion are used to verify the analytical model. The results indicate that the entrainment model is able to capture the mechanism of erosion and it can be used in the calculation of the rate of erosion for granular material. The analytical entrainment model is incorporated into a runout model to study a rock avalanche occurred on April 9, 2000 at Yigong Tibet, China. During entrainment, it is considered that the total mass is changing due to basal erosion. In addition, the profile of the channel bed is adjusted accordingly due to erosion in each calculation step. Measurements obtained from site investigation, including deposition depth and flow height at specific location, are used to verify the model. It is found that the calculated runout distance and the modified deposition height agree with field observations.

KEYWORDS
debris flow, entrainment, modelling, numerical experiment, case study

1 INTRODUCTION

Debris flows are rapid mass movement in steep hilly terrains where earthly materials flow down a valley or a channel, usually triggered by a landslide or heavy rainfall. They are usually fast-moving with variable solid concentrations and long runout distances. Due to its fast moving characteristics, debris flow is one of the most hazardous and unpredictable geological surface processes, which results in the loss of many lives and property damages (Schurch et al. 2011).

In many debris flow events, flow channels are typically covered by surficial deposits, sometimes several meters thick of loose granular material. A rapidly moving debris flow could mobilize these materials, which could change the volume of the debris flow significantly during the flow process. The inclusion of material through erosion of the flow channel is called entrainment. Many debris flows have significant amounts of entrainment, resulting in a substantially larger final volume than its initial volume, which can occupy up to 90% of the total final volume for same cases (Kang and Chan 2017).

To assess the extent of damages caused by a debris flow event, numerical modeling and debris flow analysis are often implemented. There are several approaches for debris flow modeling, including the empirical approach (Genevois and Romeo 2003; Moffat et al. 2011; Fannin et al. 2012), the discontinuum approach (Cundall and Strack 1979; Chen and Qiu 2012), and the continuum approach (Wang et al. 2010; Iverson 2012; Bouchut et al. 2016).

Various models have been developed for calculating the amount and rate of erosion in debris flow analysis (Brasil Cavalcante et al. 2013; Iverson and Ouyang 2015) (Table 1). Some efforts have been made in the past to estimate the volume of erosion and incorporate basal entrainment. The models for calculating the amount of material incorporated from channel beds can be roughly categorized into analytical models and empirical models. In the analytical approach, there are essentially two approaches to calculating entrainment: the static approach and the dynamic approach. Newton's law of motion or the force equilibrium is used to calculate the entrainment rate or depth of erosion of the channel base. Shear stress and shear resistance are the most important factors for calculating entrainment. The diffusion process caused by the difference in sediment concentration between the

erodible channel bed and the main body of the debris flow is also considered as a possible mechanism of entrainment (Iverson and Ouyang 2015). In the empirical approach, however, the entrainment rate is empirically related to the flow velocity or shear stress exerting on the erodible bed. The coefficient of correlation between the entrainment rate and flow velocity or shear stress is often determined by model calibration based on a large number of documented cases.

This paper aims to introduce a progressive scouring model and demonstrates that entrainment of granular material can be eroded by rolling motion and sliding motion. Since field laboratories cannot detect very detailed information of stress at the interface of debris and erodible bed, numerical experiment was employed to validate the entrainment model. Yigong rock avalanche was used to verify the progressive scouring entrainment runout model, in which the progressive scouring entrainment model was incorporated into an energy based runout model.

Table 1 Summary of disadvantages and advantages of different approaches in entrainment calculation (revised from Kang and Chan 2017)

Approaches	Physics	Complexity	Determination of material parameters	Range of applications	Pore pressure	Application in case histories	References
Static	Shear failure of erodible material based on shear failure	Easy	Conventional geotechnical tests	All types of soil	Y	N/A	Medina et al. (2008a);
Dynamic	Shear failure of erodible material based on rate of shear failure	Easy	Conventional geotechnical tests	All types of soil	Y	Font de la Llum event; Cardemeller debris flow; 2003 Faucon debris flow;	Medina et al. (2008b); Luna et al. (2012); Iverson and Ouyang (2015); Bouchut et al. (2016);
Diffusion process	Difference of solid concentration between flow and erodible bed	Complex	Geotechnical tests and hydraulic tests	Non-cohesive soil	N	Used in flume experiments;	Egashira et al. (2001);
Empirical approach	Correlate the rate or erosion with average flow velocity and shear stress from runout analysis	Easy	Statistical data	Soil properties generally is not considered	Y	Fjæland debris flow; The 1999 Nomash River landslide;	De Blasio et al. (2011); McDougall and Hungr (2005);
Progressive scouring	Rolling and sliding motion	Easy	Conventional geotechnical tests	Granular material	N	Yigong rock avalanche	Kang et al. (2017)

2 PROGRESSIVE ENTRAINMENT MODEL

Kang and Chan (2017) compared the force required for initiating rolling and sliding motions, and found that neglecting rolling motion could result in an underestimation of the rate of erosion, since the required force for rolling motion is less than that for sliding motion for many cases. Therefore, a particle scale entrainment model is developed to capture this erosion characteristic.

In the entrainment model, granular particles lying on channel bed are eroded by rolling and sliding (Kang and Chan, 2017). In the model, irregular granular particles are represented by uniform size sphere (disk in the case of analysis). According to analysis carried out by Wu and Chou (2003), Cheng et al. (2003) and Shodja et al. (2003), the drag force to initiate rolling action is normally less than that required for basal shear failure. Therefore it is considered that rolling motion is the dominant mechanism in the initial stage of entrainment for granular material. However both rolling and shearing motions should be considered in the calculation of entrainment rate.

In calculating the drag force for the initiation of the rolling action, it is assumed that a particle will rotate around a point O as shown in Figure 1. Drag forces arising from the moving debris above the bed are assumed to apply at the center of the particle. It is assumed that the particle will rotate around the contact point with the adjacent particle located downstream. Newton's Law of Motion is applied to calculate the acceleration, velocity, and displacement of the particle. The equation governing the motion can be written as:

$$\frac{TR}{\left(I+mR^2\right)}sin\alpha_t-\frac{mgR}{\left(I+mR^2\right)}\cos\left(\alpha_t+\theta\right)=\frac{\partial^2\alpha_t}{\partial t^2} \quad [1]$$

where T is the drag force required to initiate rolling, R is the characteristic particle size, I is moment inertial which is equal to $mR^2/2$, L = 1m for 2D, m is the mass of the particle (for 2D, $m=\pi R^2\rho_b$), ρ_b is the density of bed sediment particle, α_t is the angle between channel bed and connection line of centers of those two particles, θ is the slope angle, g is the gravity acceleration, $\partial^2\alpha_t/\partial t^2$— angular acceleration and t is time.

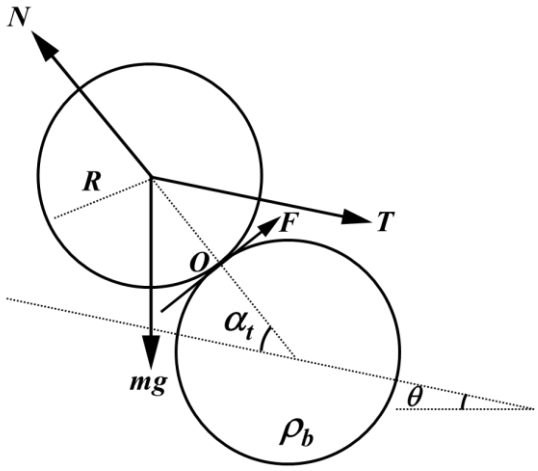

Figure 1 Illustration of forces acting on an eroding particle

It is also assumed in the derivation that once the particle moves over the adjacent particle located downstream, it will become a part of the flowing debris (Kang and Chan 2017). The entrainment rate is defined as the height of particle exposed to the flow divided by the time needed for it to be eroded. Therefore for different α_0, the initial condition of α_t, entrainment rate, $\dot{E}_i$, is defined as:

$$\dot{E}_i=\frac{2R\sin\alpha_{0i}}{t_i} \quad [1]$$

where t_i is the time required for one particle to roll from its initial position, α_0, to vertical line at which α_t equals ($\pi/2-\theta$), because it was assumed that once the particle moves over another particle, it will be a part of debris flow. Therefore, for a given shear force applied on the particle, t_i, can be determined from equation [1]. When the shear force applied on the particle is larger than the friction at the particle contact, the entrainment mode changes from rolling motion to sliding motion.

Since α_0 varies considerably in the granular assembly and it is not easy to determine individual angles at each particle contact, a statistical approach is used to provide an estimate on the values and variations of α_0. The variation of α_0 can be approximated using a probability density function (*PDF*). The model parameters for a *PDF* have significant effects on the calculations of entrainment (Kang and Chan 2017). Strictly speaking, parameters such as the mean value of the normal distribution function would be possible to measure on site (Fenton and Abbott 1977), but it only can apply to the site where the test was made. It can also be estimated using the correlation between void ratio and internal friction angle, and the correlation between particle protrusion and void ratio (Okada et al. 2007). The overall entrainment rate $\dot{E}$ can be determined from individual particle entrainment rate $\dot{E}_i$ and the probability density function P_i as:

$$\dot{E}=\sum_{i=1}^{n}(\dot{E}_i P_i) \quad [2]$$

where n is the number divisions of the probability density function in the approximation over the range of the values of α_0. For instance, if the increment of α_0 is 1 degree from 0 to 90 degrees, n will be equal to 91.

3 NUMERICAL EXPERIMENT

To simulate the entrainment process, an idealized model with debris and erodible bed channel is constructed using PFC2D (Kang and Chan 2018) (Figure 2). The model consists of three sections: acceleration section, erosional section and deposition section (Table 2). The acceleration section is to provide sufficient kinetic energy when the particle reaches the erosional section. The erosional section, 0.15 m in depth, is the key part of this experiment, which consists of frictional particles with diameter ranging from 3 mm to 4 mm, the same as the particles in the tank. Finally, these particles are deposited at deposition zone. Since cohesionless particles are used here, parallel and contact bonds does not exist between them. Model parameters and material properties are summarized in Table 3.

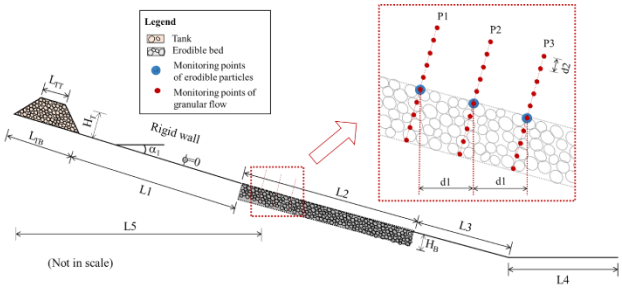

Figure 2: Geometrical sketch of the idealized model considered in the study (adapted from Kang and Chan 2018)

Table 2: Geometrical parameters of the slope and tank

Parameters	Value	Parameters	Value
α_1 (°)	15	d1 (m)	0.2
L1 (m)	3	d2 (m)	0.0375
L2 (m)	2	LTT (m)	0.3
L3 (m)	3	LTB (m)	0.6
L4 (m)	2	HT (m)	0.3
L5 (m)	4	HB (m)	0.15
Particle size (m)	0.003~0.004	Density of particles (kg/m^3)	2600

Table 3: Parameter setup in modelling (for channel bed and tank)

Items		Microscopic mechanical parameters of PFC model
Particle size	Maximum radius (m)	0.004
	Minimum radius (m)	0.003
	PDF	Uniform distribution
Particle density (kg/m^3)		2600
Porosity		0.2
Particle normal stiffness (N/m)		1e9
Particle shear stiffness (N/m)		1e9
Contact bond normal and shear strengths		0
Ball-ball friction		0.6
Ball normal stiffness (N/m)		1e10
Ball shear stiffness (N/m)		1e10
dt scale		1e-5
Local damping coefficient		0
Viscous damping coefficient (normal)		0.3
Viscous damping coefficient (shear)		0

3.1 Simulation results

To test the effects of entrainment on debris flow runout, particles located as specified locatiions are monitored (Figure 2). The runout distance and the velocity of the debris flow are obtained by monitoring moving and stationary particles in the flow channel. Shear stresses inside the measurement circles are monitored. To obtain entrainment rate dynamically, stresses and variations of the height at the interface between moving and stationary particles are calculated.

3.1.1 Average velocity and total volume

During the simulation process, average velocity and total volume are calculated. The average velocities of all moving particles are calculated. The total volume is defined as the volume of all particles mobilized. Figure 3 shows the calculated velocity and total volume. The average velocity increases linearly until the moving particles reach the erodible bed. The maximum velocity, around 2.10 m/s, occurs at the beginning of entrainment process. After that, the average velocity decreases continuously until t= 4.5s. Variation of the total volume of the moving particles starts at t = 3.2s. Therefore, the analysis of simulation results is focused on the velocities and total volume in the shaded region, between t = 3.2s and t = 4s, as shown in Figure 3.

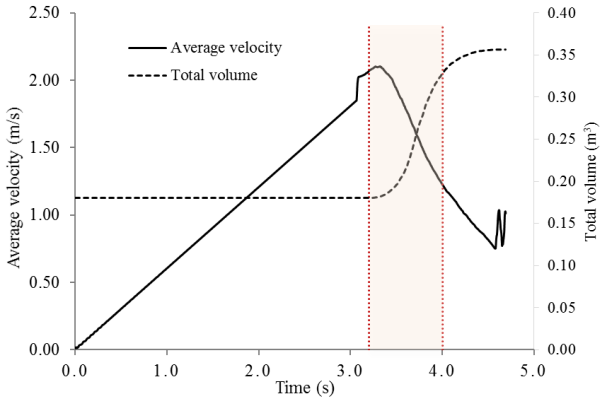

Figure 3: Average velocity of moving particles (Kang and Chan 2018)

3.1.2 Rotational velocities

Figure 4 shows the calculated rotational velocity of the particles closest to monitoring points at the erodible channel surface. These particle are selected at the initial stage of the numerical experiment and the rotational velocities are tracked throughout the flow process. Physically, particles closest to the surface of the erodible channel at P1 are moved first and then particles at P2 and P3 are moved subsequently. Positive value indicates counterclockwise rotation according to the default setting in PFC2D. The time when particles start to rotate agrees with the time when erosion starts. It means that the rotational velocities correspond to physical analysis though negative rotational velocities observed that are probably caused by particles climbing over the monitored particles.

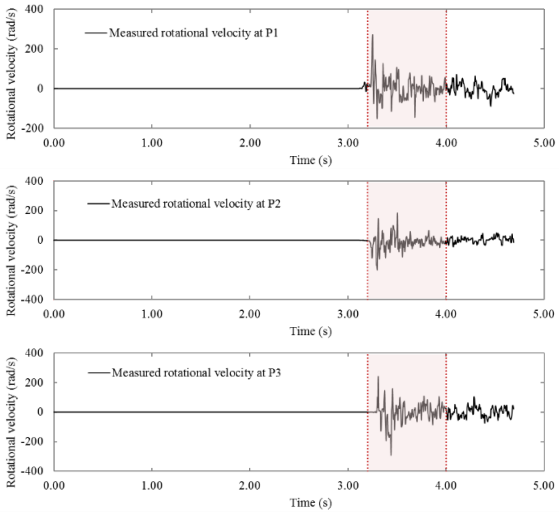

Figure 4: Variation of rotational velocities of particles at monitoring points (Kang and Chan 2018)

Figure 5 shows the distribution of x-velocity, rotational velocity and shear stress in the granular flow during the flowing process along the cross sections. Since friction

dominates the properties of granular flow, which is different from viscous flow in which viscosity dominates flow characteristics, being that highest x-velocity appears at the top of the flow channel, notably at B1 and C1. At A1, due to the boundary effect, x-velocity of particles near the initial erodible surface is smaller than that below the initial erodible surface, however in B1 and C1, the calculated x-velocity is almost linearly distributed similar as simple Couette flow.

The rotational velocity at the monitored sections varies considerably between positive and negative values with depth. Since particles override each other, the underlying particles requires larger force to move than the particles above. When the upper particle rolls forward, counter clockwise rotation, the lower particle then rolls backward, clockwise rotation, due to friction at the contact. This results in rapid changes in the direction of rotation between positive and negative values with depth.

Shear stresses also vary along the cross sections. However shear stresses increase from top to bottom in the moving particles. Since stresses are calculated using average values in a volume depending on porosity, it is expected that shear stresses will vary a little bit along the cross sections.

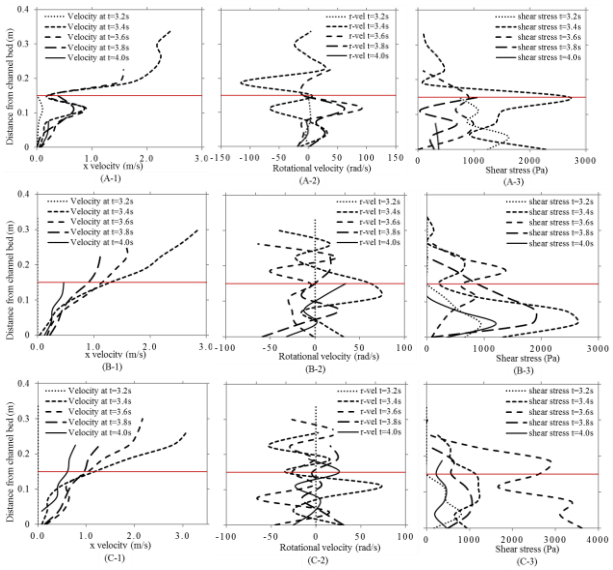

Figure 5: Flow properties along monitored cross sections (A-1, B-1 and C-1 are monitored x-velocity along cross sections P1, P2 and P3. A-2, B-2 and C-2 are monitored rotational velocity along cross sections P1, P2 and P3. A-3, B-3 and C-3 are monitored shear stress along cross sections P1, P2 and P3, which have been transformed to the direction parallel to flow channel) (Kang and Chan 2018)

3.1.3 Verification of the rate of erosion

The rate of erosion is calculated by dividing the depth of erosion by the time. The progressive scouring entrainment model is verified by comparing the entrainment rate between progressive scouring entrainment model and the PFC results. Figure 6 indicates the entrainment rates calculated using the progressive scouring entrainment model and using PFC. The deviation of entrainment rate calculated can be explained by the errors in identifying the erosion depth in discrete model which is different from continuous model.

The calculated rate of erosion from the progressive scouring entrainment model at P1 varies between 0.13 m/s and 0.21 m/s, while the entrainment rates of the other two lines change almost evenly along the diagonal line. By monitoring the entrainment process at P1, it is found that the boundary effect has an impact on the entrainment calculation since the height of moving mass is probably overestimated which is used to calculate the shear stress in the progressive scouring entrainment model. It is because some of the particles at the top part of the flow are not fully contacted with underlying particles in PFC model. These particles do not develop shear stress on the flow channel.

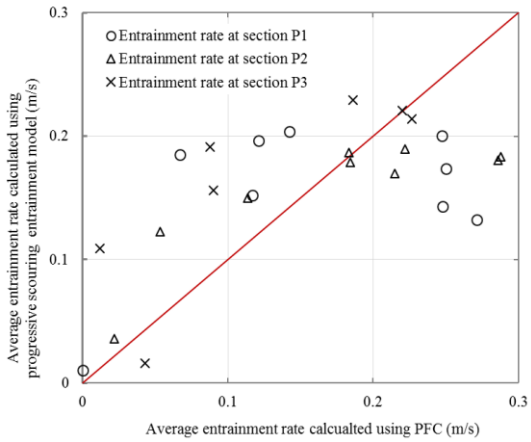

Figure 6: Comparison of entrainment rate between progressive entrainment model and PFC2D simulation (Kang and Chan 2018)

4 FIELD CASE STUDY

4.1 Case description

On April 9th 2000, a rock avalanche occurred at Yigong, Tibet, China (Figure 7). This event is considered as one of largest non-seismic mass movement in recent years (Zhang and Yin 2013). The Yigong rock avalanche (YRA) is located near Zamu Creek, a tributary of the Yigong River (Lv et al. 2002). Zamu Creek is a typical channeling valley. The slopes of its lateral mountains are between 30° and 35°. The bottom width of the creek is between 50 m and 150 m (Zhang 2013). The elevation at the source zone of the rock avalanche is about 5,350 m, and the elevation of the Yigong River bed is about 2,188m (Figure 8) (Wang 2006). The runout path is plotted in Figure 8 denoted by line P-P', which is also the profile line used in the current simulation.

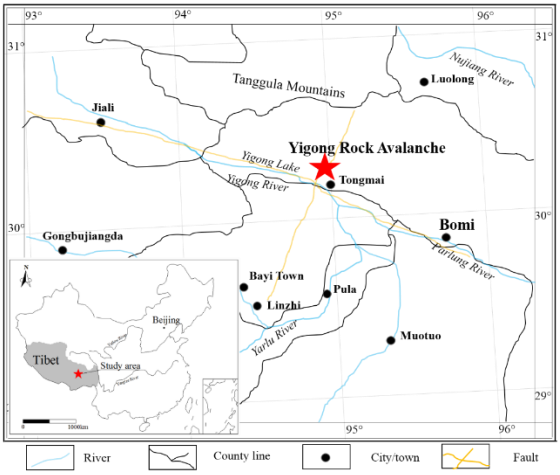

Figure 7: Geographical location of Yigong rock avalanche (revised from Kang et al. 2017)

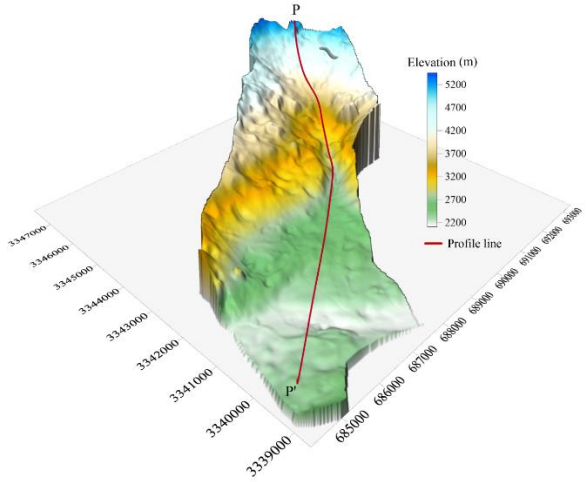

Figure 8: Digital elevation model of Yigong Rock Avalanche (Kang et al. 2017)

During the sliding process, drag forces exerted by the sliding debris could erode materials lying on the channel bed. This process could increase the final deposition volume and increase the velocity of the moving debris. The entrainment zone in Zamu Creek is mainly composed of loose colluvial materials, distributed not only on the creek banks, but also on the channel bed. Erodible material in Zamu Creek is mainly located at an elevation between 3000m and 4000m.

The deposition zone consists of boulders moved from the source area and loose debris materials in the entrainment zone. In this region, particle size changes from the central area to deposition boundary. The accumulated debris at the central area in the deposition zone composes mostly of bounders having a diameter over 3 m, and the total volume of the boulders is around 30×10^3 m^3.

Elevation variation of Zamu Creek before and after YRA is shown in Figure 9. It seems that the maximum elevation variation is around 500 m which is larger than that reported by Wang (2006). The digital elevation model used to plot the elevation variation map is based on survey a few month after the event. Snow melt and other topographic evolution process may introduce errors in the elevations.

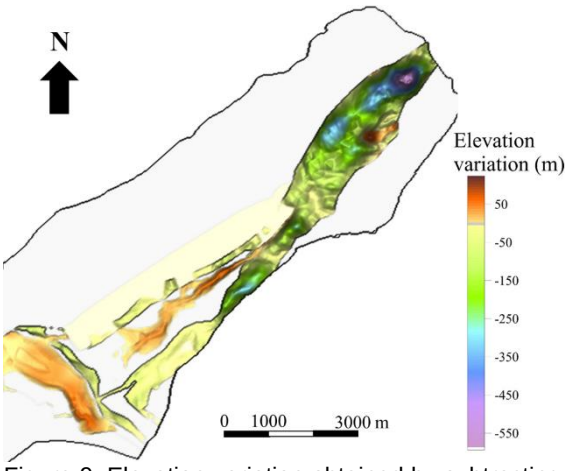

Figure 9: Elevation variation obtained by subtracting DEM after event from that before event (Kang et al. 2017)

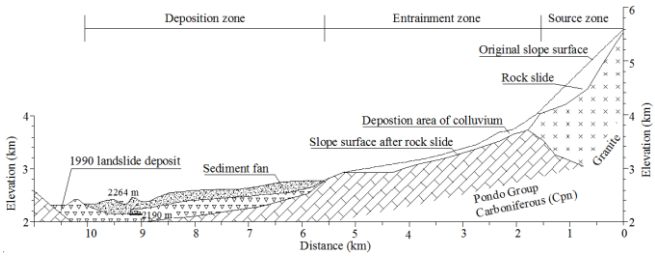

Figure 10: Longitudinal profile along YRA path (Kang et al. 2017)

4.2 Numerical simulation

According to the data collected in the field, granular particles deposited at the rock avalanche fan mainly came from the source area and transported from the entrainment zones. If the entrainment zone is close to the deposition fan and rock fragmentation has not taken place, particles located in the entrainment region should be about the same size as those in the deposition zone. Although samples can be collected in the deposition fan, it is very difficult to conduct sieve analysis since the particle ranges from very fine (clay) to very large (boulder). Therefore, a practical way to estimate the characteristic size of the material is to analyze the composition of the material. According to the description of the loose material at the deposition area (Xu et al., 2012) and particle size distribution curve obtained from the laboratory test, it is estimated that the characteristic size of the erodible material is around 300 mm.

Since it is nearly impossible to measure α_0 for all particles in place, an indirect method to estimate the mean of normal distribution is used here. The value of α_0 may be obtained from the pivoting angle and the slope angle. In the

simulation, the pivoting angle of the angular particle, ϕ_p, is estimated using the empirical relationship from Li and Komar (1986). The average slope angle can be obtained from the digital elevation model. Based on the results of sensitivity analyses, the standard deviation is found to be equal to 0.1 for this case. When the particles are eroded, close-packed particles mobilized and becomes loose. Porosity of the eroded material increase. This will cause the expansion of the material. Based on the Law of Conservation of Mass, a bulking factor is defined as ratio between the density of the material in the channel bed and the density of the debris. In the calculation, the volume of the eroded material in the debris is equal to the volume before it is eroded times the bulking factor.

The Voellmy model is used to calculate the shear stress exerting on channel bed. Xu et al. (2012) used the friction angles ranging from 0.52º to 20º on different longitudinal sections of YRA based on the calibration. Since the model is developed based on dry granular flow, a lower friction angle and basal friction angle are suggested to offset the effect of water on the soil friction. An internal friction angle of 13º and basal friction angle of 12º were used in the simulation which is smaller than that used by Xu et al. (2012). A turbulent coefficient of 500 m/s^2 is adopted in the simulation which is a little bit larger than the medium value suggested for rock avalanche (Luna et al. 2012), but it is still within the reasonable range of values. Parameters used in the simulation are summarized in Table 4.

Table 4 Parameters in the simulation

Run-out model parameters	Values
Unit weight (kN/m^3)	20
Internal friction angle (°)	13
Basal friction angle (°)	12
Turbulent coefficient (m/s^2)	500
Entrainment model parameters	
Particle size d_{50} (mm)	300
Standard deviation of α_o (°)	0.1
Mean value of α_o (°)	12
Particle density (kg/m^3)	2600
Bulking factor	1.3

The longitudinal profile shown in Figure 10 is divided into three zones from top to bottom: source zone, entrainment zone and deposition zone. In the simulation, the original slope surface changes due to entrainment in the central part of the profile. Based on the observed source volume and area of source material in 2D, a uniform width, 173 m, is calculated which is kept constant in the simulation. The number of slices could impact the calculation results. To investigate the sensitivity of the number of slice on the model results, the source material is divided into 50 slices in another run. The difference in runout distance, velocity and total volume are 0.6%, 0.1% and 1%, respectively. After evaluating the required time for the calculation and resolution of calculated results, the model with 30 slices is adopted.

4.3 Simulation Results

4.3.1 Results of runout and entrainment analyses

In the simulation, the front velocity of the rock avalanche was calculated. The calculated front velocity of YRA increases in the first 30 seconds and then gradually drops when the material reaches a relatively flat area as shown in Figure 10. A plot of the velocity versus path distance is shown in Figure 11. The maximum velocity occurs at a path distance around 3,500 m. At about 140s, the front of the debris almost stops moving but the remaining part keep moving at a very small velocity.

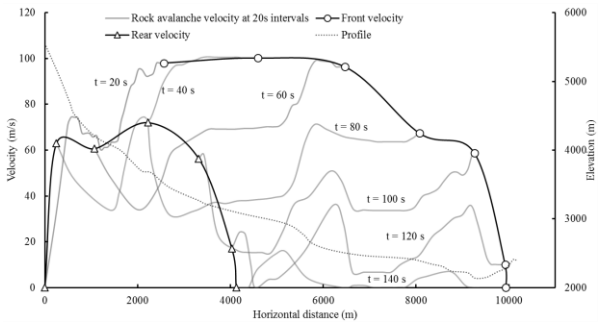

Figure 11: Velocity and its variation in the simulation (Kang et al. 2017)

Since YRA has a large initial volume travelling at high velocity, the entrainment rate is expected to be very large. The entrainment depth is assumed to be 280 m in the runout analysis using DAN (Zhang 2013). The entrainment rate of each slice at different times in this simulation is shown in Figure 12. The maximum entrainment rate is 1.79 m/s at the initial stage (Figure 13). The entrainment rate increases after 100s since the accumulated flow height has increased. This is an important drawback in 2D analysis. In the first half of the analysis, the entrainment rate increases to 1.7 m/s rapidly varying between 1-2 m/s before the debris stops moving. The maximum height of the rock avalanche decreases with time until the front suddenly reaches the flat area. The calculated maximum height of debris in the deposition area is about 320 m. The calculated maximum entrainment depth is 108 m located at x=4,218 m (Figure 14).

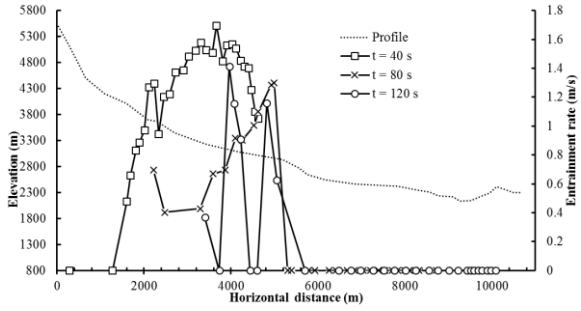

Figure 12: Entrainment rate along the channel at different time stage (Kang et al. 2017)

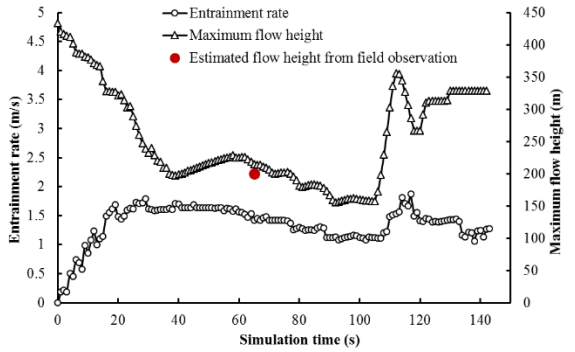

Figure 13: Maximum entrainment rate and flow height in the simulation of 2000 Yigong Rock Avalanche (Kang et al. 2017)

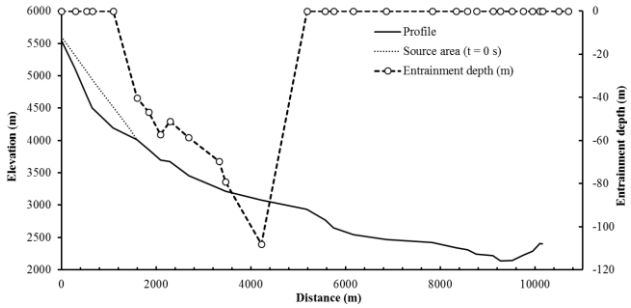

Figure 14: Calculated entrainment depth along the channel (Kang et al. 2017)

The initial volume of the debris starts at 90×10^6 m^3 and increases gradually until the front has moved about 10 km (Figure 15). When the front has almost stopped, the total volume is still increasing due to the entrainment in the tail region. The maximum increase in volume of 1.03×10^6 m^3 occurs at a run-out distance of about 5,161 m. The front velocity at that location is higher than 100 m/s. The calculated accumulated volume is not as large as that observed in the field due to neglecting bank entrainment and broadening of flow channel in the entrainment zone.

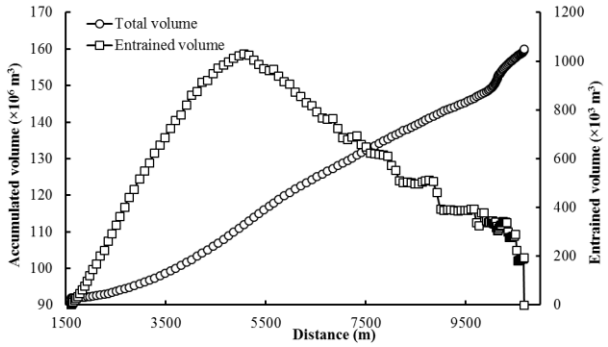

Figure 15: Entrainment volume and total volume in the simulation (Kang et al. 2017)

4.3.2 Validation of modelling results

Validation of the runout and entrainment model is based on field observations such as the estimated runout distance and deposition height. Also, results from published literature are used in evaluating the model. In the model the calculated runout distance is about 10 km which matches field observation. Since the width of the flow channel doesn't change a lot in the entrainment zone, based on the volume of the debris, the depth of entrainment can be calculated. The calculated entrainment depth is the change in the elevation of the points in the channel bed in the calculation, which is adjusted to the direction perpendicular to the slope surface. The observed depths of entrainment versus the calculated values at entrainment zone with a 100m interval are shown in Figure 16.

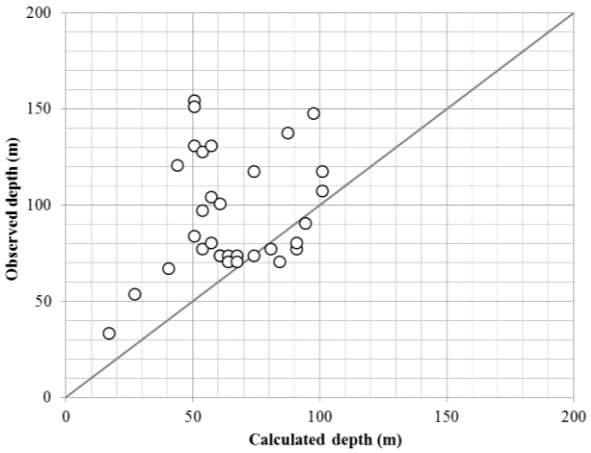

Figure 16: Comparison between observed entrainment depth in field after event and calculated entrainment depth (Kang et al. 2017)

To compare the calculated final height of the depositional fan in 2D with field observation which is in 3D, the calculated depositional height has to be adjusted to represent the field situation. A correction coefficient, C_{LS}, for lateral spreading is defined as

$$C_{LS} = W_{model} / W_{fan} \quad [3]$$

where W_{model} and W_{fan} are, respectively, the channel width in the model and the width of deposition fan. W_{model} which is the width of the channel calculated by dividing the total volume of source material by total area of source material in the 2D profile; W_{fan} is the average width of the deposition fan. A volume and height (h_{fan}) relationship and volume and width (W_{fan}) relationship can be found for this area based on the digital elevation model of the deposition fan. Based on this relationship, an equivalent width (W_{model}) can be determined for a rectangular model cross section with the same debris height (h_{fan}) and the same volume. Since the debris flow channel on site is always triangle, the cross section of debris flow channel is changed to rectangle before calculating W_{fan}. The final deposition height is modified by multiplying the correction coefficient, see Figure 17. The average flow height measured using a total

station is also shown in the figure. It is seen that the modified deposition height is very close to the average value although there are some variations at some points.

YRA is described as a very rapid rock avalanche, but there are very few evidences that can directly provide a measurement of its actual velocity. From the trees destroyed by air pressure wave on two sides of the valley and the slurry attached on the trees on the top of a mountain located at left side of the outlet, it can be assumed that YRA occurred at a very high velocity. The calculated maximum velocity is around 110 m/s which agrees reasonably well with the value calculated by Zhang (2013) using DAN 3D. This is a controversial value since this is a very high velocity compared with velocity observed in other cases. Description from witness and charred tress along the channel indicated YRA has a very high flow velocity. Such high peak velocity, 81-100 m/s, has been reported by Evans et al (1989) for case of Pandemonium Creek rock avalanche.

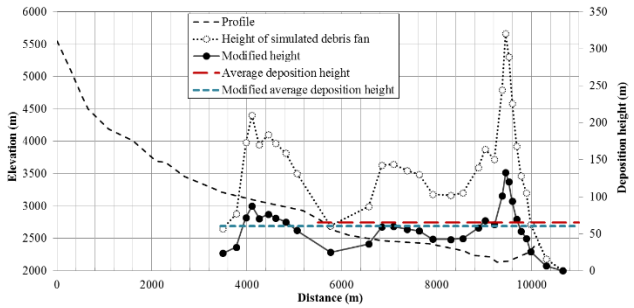

Figure 17: Modified deposition fan by taking lateral spreading into consideration (Kang et al. 2017)

5 CONCLUSION

A particle-scale entrainment model has been developed that takes into consideration both rolling and sliding motions rather than simply considering shear failure as in existing analyses. In this new model, the rate of erosion, which is equal to the available entrainment depth divided by the erosion time, is dependent on the particle size, soil density, slope angle, driving force and probable locations of two adjacent particles, estimated from the pivoting angle. Therefore, the new entrainment model can incorporate both rolling motion and sliding motion into the erosion calculation, which results in a more accurate calculation of the rate of erosion for granular material.

According to the numerical experiment, the calculated depth of erosion using the progressive scouring entrainment model is closer to the actually measured depth comparing with that calculated using the static and dynamic formulas, showing that only considering shear failure motion in erosion calculation could cause the underestimation of erosion depth.

YRA is an extremely large mass movement in recent years. The proposed scouring entrainment model calculates entrainment volume with time. This is more reasonable in considering progressive scouring since material are eroded gradually. Therefore the model can be used to simulate entrainment of channel eroded by flow at different elapsed time. Moreover channel bed elevation is adjusted after each time step to reflect changes due to entrainment which provides a more realistic simulation. This is more important in short channel with a lot of entrainment than a long channel with little entrainment.

In summary, entrainment is an important part in many debris flow runout analysis. The results from the numerical experiment and case studies reveal that the progressive scouring entrainment model has the ability to capture the primary characteristics of granular particle erosion.

ACKNOWLEDGEMENT:

This paper is supported by Opening fund of Key Laboratory of Mechanics on Disaster and Environment in Western China (Lanzhou University) (No. 201701).

Reference:

Bouchut, F., Ionescu, I.R. and Mangeney, A. 2016. An analytic approach for the evolution of the static-flowing interface in viscoplastic granular flows, *Communications in Mathematical Sciences*, 14(8), 2101-2126.

Brasil Cavalcante, A., Martins Ribeiro, L. and Pacheco de Assis, A. 2013. Experimental and Physical Modeling of Bed Load Heterogeneous Sediment Transport. *International Journal of Geomechanics*, 10.1061/(ASCE)GM.1943-5622.0000246, 545-556.

Chen, W. and Qiu, T. 2012. Numerical Simulations for Large Deformation of Granular Materials Using Smoothed Particle Hydrodynamics Method. *International Journal of Geomechanics*, 10.1061/(ASCE)GM.1943-5622.0000149, 127-135.

Cheng, N.S., Law, A.W.K. and Lim, S.Y. 2003. Probability distribution of bed particle instability, *Advances in Water Resources*, 26(4), 427-433.

Cundall, P.A. and Strack, O.D.L. 1979. A discrete numerical model for granular assemblies, *Geotechnique*, 29(1), 47-65.

De Blasio, F.V., Breien, H. and Elverhoi, A. 2011. Modelling a cohesive-frictional debris flow: an experimental, theoretical, and field-based study, *Earth Surface Processes and Landforms*, 36(6), 753-66.

Egashira, S., Honda, N. and Itoh, T. 2001. Experimental study on the entrainment of bed material into debris flow, *Physics and Chemistry of the Earth, Part C: Solar, Terrestrial & Planetary Science*, 26(9), 645-650.

Evans, S.G., Clague, J.J., Woodsworth, G.J., and Hungr, O. 1989 The Pandemonium Creek rock avalanche, British Columbia, *Canadian Geotechnical Journal*, 26(3), 427-446.

Fannin, R.J., Busslinger, M. and Jordan, P. 2012. Debris flow travel distance: Field traverse data and regional guidelines for terrain stability assessment. *Proceeding of the 11th International and 2nd North American Symposium on Landslides*, Editors: Erik Eberhardt, Corey Froese, A. Keith Turner and Serge Leroueil, Banff Canada, June 3-8, 2012, Balkema, Taylor and Francis Group, London, 1: 751-756.

Fenton, J.D. and Abbott, J.E. 1977. Initial Movement of Grains on a Stream Bed: The Effect of Relative Protrusion, *Proceedings of the Royal Society of London Series a-Mathematical Physical and Engineering Sciences, The Royal Society*, 352(1671), 523-537.

Genevois, R. and Romeo, R. 2003. Probability of Failure Occurrence and Recurrence in Rock Slopes Stability Analysis. *International Journal of Geomechanics*, 10.1061/(ASCE)1532-3641(2003)3:1(34), 34-42.

Iverson, R.M. 2012. Elementary theory of bed-sediment entrainment by debris flows and avalanches, *Journal of Geophysical Research*, 117, F03006, doi:10.1029/2011JF002189.

Iverson, R.M. and Ouyang, C. 2015. Entrainment of bed material by Earth-surface mass flows: Review and reformulation of depth-integrated theory, *Reviews of Geophysics*, 53(1), 27-58.

Kang, C. and Chan, D. 2018. Numerical simulation of 2D granular flow entrainment using DEM, *Granular Matter*, 20(1), https://doi.org/10.1007/s10035-017-0782-x.

Kang, C. and Chan, D. (2017). Modelling of entrainment in debris flow analysis for dry granular material. *International Journal of Geomechanics* (ASCE), 17(10), 1-20.

Kang, C., Chan, D., Su, F. and Cui, P. 2017. Runout and entrainment analysis of an extremely large rock avalanche—a case study of Yigong, Tibet, China, *Landslides,* 14(1), 123-139.

Li, Z.L. and Komar, P.D. 1986. Laboratory measurements of pivoting angles for applications to selective entrainment of gravel in a current, *Sedimentology*, 33(3), 413-423.

Lv, J.T., Wang, Z.H. and Zhou, C.H. 2002. A tentative discussion on the monitoring of the Yigong landslide-blocked lake with satellite remote sensing technique, *Acta Geoscience Sinica*, 23(4), 363-368. (In Chinese).

McDougall, S. and Hungr, O. 2005. Dynamic modelling of entrainment in rapid landslides, *Canadian Geotechnical Journal*, 42(5), 1437-1448.

Medina, V., Bateman, A. and Hurlimann, M. 2008a. A 2D finite volume model for bebris flow and its application to events occurred in the Eastern Pyrenees, *International Journal of Sediment Research*, 23(4), 348-360.

Medina, V., Hürlimann, M. and Bateman, A. 2008b. Application of FLATModel, a 2D finite volume code, to debris flows in the northeastern part of the Iberian Peninsula, *Landslides*, 5(1), 127-142.

Moffat, R., Fannin, R.J. and Garner, S.J. 2011. Spatial and temporal progression of internal erosion in cohesionless soil, *Canadian Geotechnical Journal*, 48(3), 399-412.

Okada, Y. and Ochiai, H. 2007. Coupling pore-water pressure with distinct element method and steady state strengths in numerical triaxial compression tests under undrained conditions, *Landslides*, 4(4), 357-369.

Quan Luna, B. Q., Remaitre, A., van Asch, T. W. J., Malet, J. P. and van Westen, C. J. 2012. Analysis of debris flow behavior with a one dimensional run-out model incorporating entrainment, *Engineering Geology*, 128, 63-75.

Schurch, P., Densmore, A.L., Rosser, N.J. and McArdell, B.W. 2011. Dynamic controls on erosion and deposition on debris-flow fans, *Geology*, 39 (9), 827-830.

Shodja, H. M. and Nezami, E. G. 2003. A micromechanical study of rolling and sliding contacts in assemblies of oval granules, *International Journal for Numerical and Analytical Methods in Geomechanics*, 27(5), 403-424.

Wang, X.B., Morgenstern, N. and Chan, D. 2010. A model for geotechnical analysis of flow slides and debris flows, *Canadian Geotechnical Journal*, 47(12), 1401-1414.

Wang, Z.H. 2006. Large scale individual and slide remote sensing, *Earth Science Frontiers*, 13(5), 516-523. (In Chinese).

Wu, F.C. and Chou, Y.J. 2003. Rolling and Lifting Probabilities for Sediment Entrainment, *Journal of hydraulic engineering*, 129(2), 110-119.

Xu, Q., Shang, Y.J., van Asch, Th.W.J., Wang, S.T., Zhang, Z.Y. and Dong X.J. 2012. Observations from the large, rapid Yigong rock slide-debris avalanche, southeast Tibet, *Canadian Geotechnical Journal*, 49(5), 589-606.

Zhang, M. and Yin, Y.P. 2013. Dynamics, mobility-controlling factors and transport mechanisms of rapid long-runout rock avalanches in China, *Engineering Geology*, 167, 37-58.

Zhang, Y.J. 2013. Study on dynamic characteristics of typical rock avalanches on canyon area (*Master's thesis*), Shanghai Jiaotong University, Shanghai, China. (In Chinese).